PHYSICAL REVIEW A VOLUME 22, NUMBER 5 NOVEMBER 1980

# Influence of broadband photocoupling on $K$-shell excitation in aluminum

K. G. Whitney
*Optical Sciences Division, Naval Research Laboratory, Washington, D. C. 20375*

J. Davis
*Plasma Radiation Group, Naval Research Laboratory, Washington, D. C. 20375*

J. P. Apruzese
*Science Applications, Inc., McLean, Virginia 22102*
(Received 11 September 1979)

A detailed theoretical model of the collisional and radiative couplings within the aluminum $K$ shell is described which has been used to self-consistently calculate the functional dependence of the excitation state of the $K$ shell and its emission spectrum on ambient plasma conditions for a wide range of $K$-shell opacities. Both line and continuum couplings are included in the model over a range of photon energies from 442 eV to 6.13 keV. The approach of the interior of the aluminum plasma to local thermodynamic equilibrium has been investigated for millimeter sized plasmas where the $K$-shell couplings are photodominated and the plasma interior must come into radiative equilibrium. The approach of the $K$-series emission spectrum, which includes satellite and intercombination lines of the heliumlike resonance line, to the blackbody curve is computed. Temperature variations of the power output in continuum and line radiation are also computed and discussed. Finally, a set of calculations that relate to the ability of an external source of x radiation to selectively photopump the $3p$ state and maintain an inversion between $2p$-$3d$ levels within the heliumlike ionization stage is described. Two important effects are seen. One, the opacity of the heliumlike $L\alpha$ line plays an important role in determining the ability of the external radiation to invert levels within the plasma interior, and two, the inversion saturates with increasing pump strengths as the heliumlike ground-state population is depleted by the pump.

## I. INTRODUCTION

In the gray-body approximation of radiation transport theory,[1] the detailed atomic structure of the radiating medium is, by definition, ignored so that the absorption coefficient over the broadband of the emitted radiation can be taken to be frequency independent. As a result of this assumption, appropriately frequency averaged absorption coefficients are used, the two most common being the Planck and Rosseland means corresponding to optically thin and thick physical situations, respectively, depending on the size and density of the emission region. In addition, the medium is usually restricted to be in local thermodynamic equilibrium (LTE). Then, the source function for the radiation field can be specified to be the blackbody source function, $B_\nu(T_e)$.

In this paper, we will investigate the behavior of aluminum as a broadband source of kilovolt x rays starting from a much more ambitious set of theoretical assumptions and objectives than are used in the gray-body approximation. LTE conditions will not be assumed. Rather, we shall study the approach of aluminum to LTE as a combined function of electron-ion and radiation field-ion interactions. In addition, special emphasis will be placed on the calculation of self-consistent aluminum $K$-shell emission spectra as they approach the blackbody curve. Thus, the detailed frequency dependence of both the source function and the absorption coefficient will have to be determined from a detailed treatment of the aluminum medium and vice versa. Steady-state conditions will be assumed in these calculations.

Because of the relative simplicity of one- and two-electron optical spectra, emission from the hydrogenlike and heliumlike ionization stages within the $K$ shell produces one of the simplest spectra to analyze in detail. However, even in this case, approximations must be made with respect to the amount of spectral detail and energy-level structure employed in the calculations. Nevertheless, one can be guided, as we have, by experiment in order to model either the most prominent or some of the most diagnostically important features of the $K$-shell emission spectrum. Furthermore, only through a detailed treatment of the major photocouplings and of the competing coupled emission and absorption processes can both diagnostic and dynamic information on the aluminum plasma's collisional-radiative state be self-consistently determined.

## II. IONIZATION MODEL

The $K$-shell spectrum we have chosen to compute as well as the couplings to the aluminum plasma that both produce and self-absorb this radiation are shown in Fig. 1. The spectrum consists of

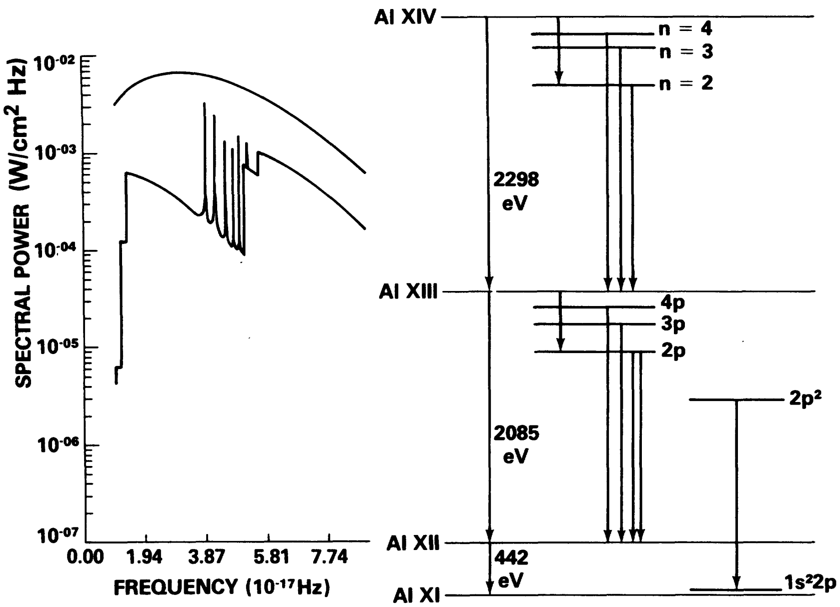


FIG. 1. The $K$-series aluminum spectrum on the left is calculated from the radiative transitions connecting the Al XI-XIV energy levels shown on the right. Also listed are the locations of the aluminum ground-state–to–ground-state radiative recombination emission edges.

five free-bound continua and eight lines whose upper ionic states lie in the hydrogenlike and heliumlike manifold of states. The spectrum begins at the emission edge of the Al XII to Al XI (He → Li) radiative recombination continuum at 442 eV and extends to 6.13 keV, far into the wings of the Al XIV to Al XIII (Z → H) and Al XIII to Al XII (H → He) recombination continua. Lyman $\alpha$-, $\beta$-, and $\gamma$-like line emission from Al XII and Al XIII is computed along with the $1s^2$-$1s2p\,^3P$ intercombination line in Al XII and the $1s^2\,2p$-$1s2p^2\,^2D$ satellite line in Al XI. These lines lie on the background continuum which is produced by the He → Li, Z → H($n$ = 2), and H → He($1s2p\,^3P$) recombinations. The H-like $L\gamma$ line also lies on the generally strong H → He continuum.

The excited-state structure of our aluminum ionization model consists only of the $K$-shell levels shown in Fig. 1 together with $1s2s\,^1S$, $1s3s\,^1S$, and $1s3d\,^1D$ states in Al XII and $2p$, $3s$, $3p$, $3d$, and $4d$ states in Al XI. Only the radiative couplings shown in Fig. 1 are included in this model, e.g., both Balmer and lithiumlike line emission are purposefully suppressed. Thus, all of our radiative couplings to the aluminum $K$ shell can be fully detail balanced as blackbody radiation energy densities within the medium are reached. As a consequence, collisional-radiative equilibrium (CRE) calculations performed with this model can sensitively model the aluminum $K$ shell's approach to LTE even under conditions where its radiative couplings are much stronger than the corresponding collisional couplings.

Because of the generally local nature of electron-ion interactions and in spite of the fact that the strength of many of the $K$-shell radiative interactions can be and often are much stronger than the corresponding strength of the collisional interactions, it has historically been the case that CRE calculations emphasize and are much fuller in their collisional than in their radiative couplings. A similar condition exists within the present state of our aluminum $K$-shell model, i.e., it contains a complete network of collisional transitions and only the partial (13) set of radiative transitions described above. The density and temperature behavior of the rate coefficients coupling the level structure in Al XI has been described in one of our earlier papers.[2] The 5 bound excited states are fully coupled collisionally to one another and to the Al XI and Al XII ground states. The $1s2p^2$ autoionizing state, on the other hand, is excited only by dielectronic recombination from the Al XII ground state. It decays radiatively to the $1s^2\,2p$ state and by autoionization with a rate of $1.41 \times 10^{14}$ sec$^{-1}$, which was computed recently.[3] The excited states within the Al XII and Al XIII ionization stages are also fully coupled collisionally. The level structure and collisional couplings for this aluminum $K$-shell model are identical to the structure and couplings that we used in a previously described carbon $K$-shell ionization model.[4]

### III. CRE EQUATIONS–PLASMA MODEL

Since we are interested in the full CRE behavior of the aluminum $K$ shell for a widely varying set of plasma conditions, the ionization dynamics and $K$-shell emission spectrum must be computed from one another self-consistently. Hence, the major computational problem is not just to solve the radiation transport equation, but to calculate a self-consistent set of photocouplings, and to relate the strength of these couplings to the calculated emission spectrum. If we let $N_a$ denote the population density of the $a$th ionization state of the plasma and $W_{ab}$ denote the total rate of the transitions from the $b$th to the $a$th state, then in CRE, $N_a$ must be determined by solving the following set of rate equations:

$$\sum_b W_{ab}(N_e, U_\nu)N_b = 0 \,, \tag{1}$$

$$\sum_b N_b = N_i \,, \tag{2}$$

and

$$\sum_b Z_b N_b = N_e \,. \tag{3}$$

$N_i$ is the total ion density, $N_e$ is the electron density, $U_\nu$, the radiation energy density at frequency $\nu$, and $Z_b$ is the ionic charge of the $b$th state. Because of the rate coefficient dependence on $U_\nu$, solutions to Eqs. (1)–(3) are geometry dependent. In a planar geometry, $U_\nu$ can be calculated by solving a transport equation for the specific intensities, $I_\nu(\mu, z)$, of the form[5]

$$\mu \frac{d}{dz} I_\nu = + k_\nu (S_\nu - I_\nu) \,, \tag{4}$$

where $\mu$ is the cosine of the angle between the light ray and the normal to the plane along which $z$ is calculated. $k_\nu$ and $S_\nu$ are the absorption coefficient and source function, respectively, of the radiation at frequency $\nu$. $U_\nu$ (in units of ergs/$\text{cm}^3$ Hz) is found from $I_\nu$ by averaging over the angles of the different ray directions:

$$U_\nu(z) = \frac{2\pi}{c} \int_{-1}^{1} d\mu \, I_\nu(\mu, z) \,. \tag{5}$$

In addition the emission spectrum $W(\nu)$ (in units of erg/$\text{cm}^2$ sec Hz), is calculated from the first moment of $I_\nu$ evaluated at the surface of the plasma:

$$W(\nu) = 2\pi \int_{-1}^{1} d\mu \, \mu I_\nu(\mu, z = Z_0) \,. \tag{6}$$

The ionization and emission behavior of aluminum that is described in this paper is obtained from solutions to Eqs. (1)–(6).

Photon coupling to a set of rate equations can be carried out through the use of Einstein $A$ and $B$ coefficients, which satisfy the detail balance relations,[6]

$$B_{ab}(\nu) = \frac{A_{ab}(\nu)}{(8\pi\nu^2/c^3)h\nu} \,, \tag{7}$$

$$B_{ba}(\nu) = (N_b/N_a)_{\text{LTE}} \, e^{h\nu/kT_e} B_{ab}(\nu) \,, \tag{8}$$

where $(\;)_{\text{LTE}}$ denotes that LTE relative values of the population densities are to be taken. The $A$ coefficients can be factored into a total decay rate, $A_{ab}^T$, times a profile function $\phi_{ab}(\nu)$, where $\int \phi_{ab}(\nu) d\nu = 1$:

$$A_{ab}(\nu) \equiv A_{ab}^T \phi_{ab}(\nu) \,. \tag{9}$$

For free-bound continuum emission, $\phi$ was taken to have the form[7]

$$\phi_{ab}(\nu) = \eta_+(\nu - \nu_{ba})(h/kT_e) e^{h(\nu_{ba} - \nu)/kT_e} , \tag{10}$$

where $h\nu_{ba} \equiv E_b - E_a$ is the energy difference between the ionic states of the transition and $\eta_+$ is the Heaviside function:

$$\eta_+(\nu) = \begin{cases} 1, & \nu \geq 0 \\ 0, & \nu < 0 \,. \end{cases} \tag{11}$$

The total rate of radiative recombination, $A_{ab}^T$

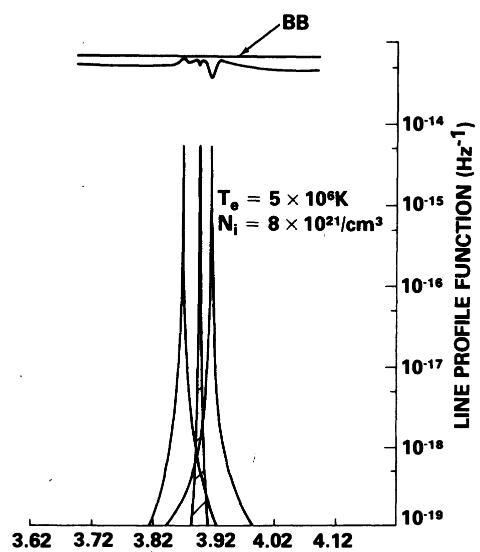


FIG. 2. On the bottom of this figure, the calculated line profile functions of the heliumlike resonance, intercombination, and satellite lines are drawn for an electron temperature of $5 \times 10^6$ K, an ion density of $8 \times 10^{21}$ cm$^{-3}$, and a 2-mm thick planar plasma. On the top of the figure, the calculated emission spectrum of these lines under these plasma conditions is compared to the blackbody curve.

$\equiv N_e\alpha_{ab}(T_e)$, was calculated using Seaton's formula,[8]

$$\alpha_{ab}(T_e)=5.2\times10^{-14}Z_b\lambda^{1/2}(0.43+\tfrac{1}{2}\ln\lambda+0.47/\lambda^{1/3}) , \tag{12}$$

where $\lambda\equiv h\nu_{ba}/kT_e$.

For line emission, energy and momentum conservation imply that $\phi_{ab}$ has the form, which is compatible with Eqs. (7) and (8):

$$\phi_{ab}(\nu)=e^{-h(\nu-\nu_{ba})/2kT_e}\,\phi^{V}_{ab}(\nu) , \tag{13}$$

where $\phi^{V}_{ab}(\nu)$ was taken in our calculations to be a Voigt profile whose collisional width was determined from the total lifetime, including stimulated emission (i.e., power broadening), of the excited state $b$.[9] Thus, at high plasma densities, where the collisional lifetime of the excited state exceeds the radiative lifetime, the Voigt parameter, $a\equiv\Delta\nu_c/\Delta\nu_D$, which is the ratio of collisional to Doppler linewidths, becomes linearly dependent on electron density. Finally, the following set of calculated values for the spontaneous radiative decay rates $A^{T}_{ab}$ were used in our calculations:

| | Transition | $A$ (sec$^{-1}$) |
|---|---|---|
| Al XIII | $n=1$-$n=2$ | $1.34\times10^{13}$ |
| | $n=1$-$n=3$ | $1.59\times10^{12}$ |
| | $n=1$-$n=4$ | $3.66\times10^{11}$ |
| Al XII | $1s^2$-$1s2p\,^3P$ | $2.54\times10^{10}$ |
| | $1s^2$-$1s2p\,^1P$ | $2.83\times10^{13}$ |
| | $1s^2$-$1s3p\,^1P$ | $7.71\times10^{12}$ |
| | $1s^2$-$1s4p\,^1P$ | $3.2\times10^{12}$ |
| Al XI | $1s^2\,2p$-$1s2p^2\,^2D$ | $1.3\times10^{13}$ |

Local photocoupling within the plasma occurs by means of Eqs. (1). The long-range, cross-coupled nature of the radiation interactions manifests itself in Eq. (4), which can be placed in the form,

$$\mu\frac{d}{d\tau_\nu}I_\nu=I_\nu-S_\nu , \tag{14}$$

where the increment $d\tau_\nu$ in optical depth is defined as $d\tau_\nu\equiv-k_\nu dz$. In general, $S_\nu$ and $k_\nu$ must be computed by summing over the various processes in which a photon at a given frequency is emitted or absorbed within the plasma. Each of the eight line profiles was calculated over a frequency interval that overlapped with the neighboring line profile. Thus, at high densities emission in the wings of one line is partially reabsorbed by and pumps the line nearest it in the spectrum. The greatest overlap of line and continuum processes, however, occurs in the vicinity of the resonance, intercombination, and satellite triplet of lines. Their overlapping line profiles are drawn in Fig. 2 at an aluminum ion density of $8\times10^{21}$ cm$^{-3}$ and at an electron temperature of $5\times10^{6}$ K. As an illustration of the net outcome of this line coupling, a calculated emission spectrum is shown above the line profiles in comparison to the $5\times10^{6}$ K blackbody emission curve. In the vicinity of these lines $k_\nu$ and $j_\nu\equiv k_\nu S_\nu$ must be calculated by summing over the different line and continuum processes that couple in this frequency interval:

$$k_\nu=k^{\mathrm{RL}}_\nu+k^{\mathrm{IL}}_\nu+k^{\mathrm{SL}}_\nu+k^{\mathrm{C}}_\nu , \tag{15}$$

$$j_\nu=j^{\mathrm{RL}}_\nu+j^{\mathrm{IL}}_\nu+j^{\mathrm{SL}}_\nu+j^{\mathrm{C}}_\nu , \tag{16}$$

where the superscripts, RL, IL, SL, and C denote resonance line, intercombination line, satellite line, and continuum, respectively. The continuum absorption and emission coefficients are, in turn, sums over the three free-bound transitions in Fig. 1 that radiate into the frequency interval around this triplet of lines. Finally, self-consistency with the photocouplings in Eqs. (1) requires that the individual absorption and emission coefficients be related to the Einstein $A$ and $B$ coefficients by the expressions

$$(k_\nu)_{ab}=(h\nu/c)[B_{ba}(\nu)N_a-B_{ab}(\nu)N_b] , \tag{17}$$

$$(j_\nu)_{ab}=(h\nu/4\pi)A_{ab}(\nu)N_b . \tag{18}$$

In solving Eqs. (1)–(18), we made no attempt to fully resolve the spatial variations of the population and radiation energy densities that are introduced by their mutual interactions even under the assumptions we made that the plasma had a uniform total ion density and uniform electron and ion temperatures. Nevertheless, the calculations generated a good deal of information about the aluminum plasma's radiative behavior. Moreover, they were self-consistent and demonstrated important effects of the induced spatially varying photocouplings. In all, in the calculations that were performed, a symmetric plasma problem was assumed, half of the plasma was divided into 11 cells, and the temperature dependence of 167 collisional rate coefficients was calculated along with 29 population densities, 136 radiation energy densities, and 13 photocouplings per cell.

## IV. APPROACH TO THERMODYNAMIC EQUILIBRIUM

In order to reach thermodynamic equilibrium, the combined ionic radiation system must satisfy this condition: the population densities must attain their LTE values ($N^*_a$) enabling the source function to reach blackbody values,

$$B_\nu(T_e)=\frac{2h\nu^3/c^2}{e^{h\nu/kT_e}-1} . \tag{19}$$

If we focus our attention, for example, on an excited state of the plasma of population density $N_u$ which undergoes a radiative transition to a lower lying state having a population density $N_l$, then, in general, in collisional-radiative equilibrium,

$$(W^{\mathrm{CD}}+W^{\mathrm{PD}}+W^{\mathrm{OD}})N_u=(W^{\mathrm{CE}}+W^{\mathrm{PE}})N_l+\sum_{p(p\neq l)}W_pN_p\,. \tag{20}$$

In this equation, $W^{\mathrm{CE}}$, $W^{\mathrm{CD}}$, $W^{\mathrm{PE}}$, and $W^{\mathrm{PD}}$ denote the collisional and radiative excitation and deexcitation rates, respectively, that connect states $l$ and $u$ directly. $W^{\mathrm{OD}}$ represents the sum over all rates for which $u$ deexcites to other states than $l$. Finally, $\sum W_pN_p$ represents the sum over all excitation processes of the upper state that originate from states other than $l$. We can solve Eq. (20) for the ratio of the population densities:

$$\frac{N_u}{N_l}=\frac{W^{\mathrm{CE}}+W^{\mathrm{PE}}+\sum_p W_p(N_p/N_l)}{W^{\mathrm{CD}}+W^{\mathrm{PD}}+W^{\mathrm{OD}}}\,. \tag{21}$$

Then, if one defines $b_{ul}$ to be this ratio when the plasma is in LTE,

$$b_{ul}\equiv\frac{N_u^*}{N_l^*}=\frac{W^{\mathrm{CE}}}{W^{\mathrm{CD}}}=\frac{g_u}{g_l}e^{-h\nu_{ul}/kT_e}\,, \tag{22}$$

a measure of the extent to which the plasma is out of LTE can be defined by

$$\epsilon_{ul}\equiv 1-(N_u/N_l)/b_{ul}\,. \tag{23}$$

From Eq. (21) one then finds that

$$\epsilon_{ul}=f^{\mathrm{PD}}(1-s^P/b_{ul})+f^{\mathrm{OD}}(1-s^O/b_{ul})\,, \tag{24}$$

where

$$f^{\mathrm{PD}}\equiv\frac{W^{\mathrm{PD}}}{W^{\mathrm{CD}}+W^{\mathrm{PD}}+W^{\mathrm{OD}}}\,, \tag{25}$$

$$f^{\mathrm{OD}}\equiv\frac{W^{\mathrm{OD}}}{W^{\mathrm{CD}}+W^{\mathrm{PD}}+W^{\mathrm{OD}}}\,, \tag{26}$$

$$s^P\equiv W^{\mathrm{PE}}/W^{\mathrm{PD}}\,, \tag{27}$$

$$s^O\equiv\sum_p\frac{N_p}{N_l}\frac{W_p}{W^{\mathrm{OD}}}\,. \tag{28}$$

Thus, the degree to which the population densities are out of LTE is given by a weighted average over the degrees to which (1) photoexcitation and deexcitation processes and (2) other quenching processes that connect to the upper level do not separately detail balance. The weighting factors are branching ratios that determine the relative strengths of the three distinguished deexcitation processes.

A similar analysis can be carried out for the source function $S_\nu$, which can be written, in general, in the form

$$S_\nu\equiv(j_\nu^L+j_\nu^C)/(k_\nu^L+k_\nu^C)\,, \tag{29}$$

where $j_\nu^L$ and $k_\nu^L$ are the total emission and absorption coefficients of the eight overlapping lines in the calculation. In an infinite, uniform medium, for example, the departure of the radiation field from that of a blackbody field can be defined in terms of the departure of the source function from $B_\nu$:

$$\epsilon_\nu\equiv 1-S_\nu/B_\nu\,. \tag{30}$$

Then, from Eq. (29), one finds that

$$\epsilon_\nu=F_\nu^L(1-S_\nu^L/B_\nu)+F_\nu^C(1-S_\nu^C/B_\nu)\,, \tag{31}$$

where

$$F_\nu^L\equiv k_\nu^L/(k_\nu^L+k_\nu^C)\,, \tag{32}$$

$$F_\nu^C\equiv k_\nu^C/(k_\nu^L+k_\nu^C)\,, \tag{33}$$

$$S_\nu^L\equiv j_\nu^L/k_\nu^L\,,$$

$$S_\nu^C\equiv j_\nu^C/k_\nu^C\,. \tag{35}$$

Thus, $S_\nu$ differs from $B_\nu$ in proportion to the amount that continuum (free-bound) or line absorption is dominant and also in proportion to the degree to which the individually defined continuum or line source functions differ from $B_\nu$.

For the $K$ shell of an optically thin aluminum plasma to be in LTE (i.e., to be collisionally dominated), the collision theory of our model predicts that the ion density must be at least $10^{24}$ cm$^{-3}$. However, in an optically thick aluminum plasma, LTE can be reached at much lower ion densities depending, to some extent, on the line profiles. In order to investigate this phenomenon, we performed the following calculation. A planar plasma, 2-mm thick, at a uniform electron and ion temperature of $5\times10^6$ K, was chosen and CRE solutions to Eqs. (1)–(18) were obtained for ion densities up to $10^{23}$ cm$^{-3}$. The total ion density was taken to be uniform. The behavior of the population densities was monitored in terms of the quantities defined in Eqs. (20)–(28). Figures 3 and 4 show, respectively, the relative progressions of the population densities of the $n=1$ and $n=2$ states of Al XIII and of the $1s^2\,{}^1S$ and $1s2p\,{}^1P$ states of Al XII towards LTE at the center of the plasma ($z=0$).

In each figure the curve labeled 1 is a plot of $\epsilon_{ul}$, curves 2 and 3, are plots of $1-s^P/b_{ul}$ and $1-s^O/b_{ul}$, respectively, the curves 4 and 5, are plots of $f^{\mathrm{PD}}$ and $f^{\mathrm{OD}}$, respectively. The population densities for the $L\alpha$ transition in Al XIII reach LTE (to better than 1%) at an ion density of $6\times10^{21}$ cm$^{-3}$, while the populations of the Al XII $L\alpha$ transition respond more slowly to the buildup in the radiation densities at the center of the plasma and require an ion density of $10^{22}$ cm$^{-3}$ to come into LTE.

Note that curves 4 and 5 cross at a higher density,

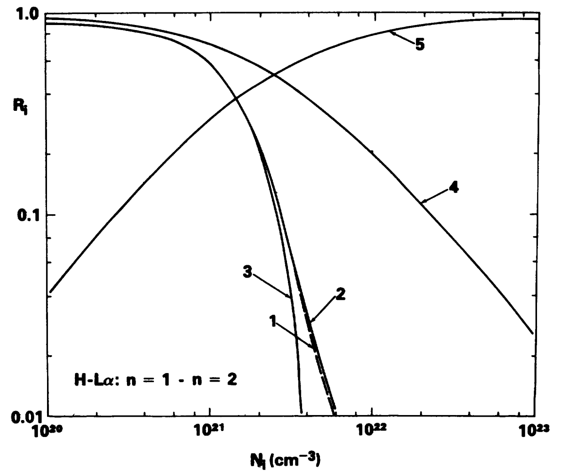


FIG. 3. The quantities appearing in Eq. (24) are computed as a function of ion density for the energy levels involved in the hydrogenlike Lyman-$\alpha$ emission. The quantities $\epsilon_{ul}$, $1-s^P/b_{ul}$, $1-s^O/b_{ul}$, $f^{PD}$, and $f^{OD}$, labeled as curves 1–5, respectively, were calculated at the center of a 2-mm thick uniform-density, planar plasma at a temperature of $5\times10^6$ K.

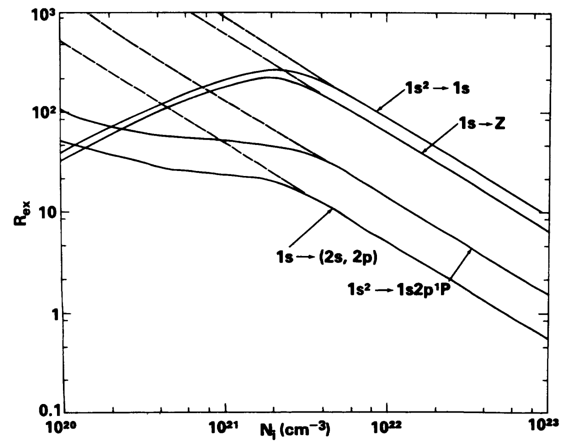


FIG. 5. Ratios of photo to collisional excitation rates (solid curves) and deexcitation rates (dashed curves) connecting upper and lower radiating states are plotted against ion density for the Lyman-$\alpha$ lines of Al XII and Al XIII as well as the Z → H and H → He ground-state radiative recombinations. These ratios were calculated at the center of a 2-mm thick, uniform-density plasma having a temperature of $5\times10^6$ K.

and after thermal equilibration has substantially occurred, in the hydrogenlike system (Fig. 3) than in the heliumlike system (Fig. 4). Thus, the influence of collisions, which connect the $2p$ states of Al XII and Al XIII to states other than the $1s^2$ and $1s$, is stronger relative to the Lyman-$\alpha$ couplings in Al XII than in Al XIII. Also, note that curves 2 and 3 fall together in both figures. Thus, the behavior of curves 2–5 suggests (1) that the

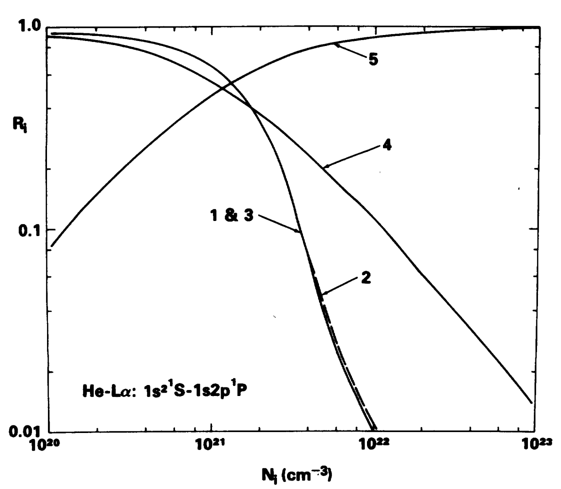


FIG. 4. The quantities appearing in Eq. (24) are computed as a function of ion density for the energy levels involved in the heliumlike Lyman-$\alpha$ emission. The quantities $\epsilon_{ul}$, $1-s^P/b_{ul}$, $1-s^O/b_{ul}$, $f^{PD}$, and $f^{OD}$, labeled as curves 1–5, respectively, were calculated at the center of a 2-mm thick uniform-density, planar plasma at a temperature of $5\times10^6$ K.

imbalance in the photorates which define $s^P$ reflects itself in an imbalance of the rate processes defining $s^O$, and (2) that the lower the density at which $f^{OD}$ exceeds $f^{PD}$, the higher will be the ion density that it takes for the population densities to reach LTE. However, for a 2-mm thick planar plasma, we see that LTE is reached at an ion density 100 times lower than is required in optically thin aluminum plasmas.

Figure 5 provides a reason for this behavior. The solid curves are ratios of photo-to-collisional excitation at the center of the plasma for the four transitions indicated. The dashed curves are corresponding ratios of photo to collisional deexcitation. The merging of the dashed and solid curves occurs at densities where the photorates begin to detail balance. In all of the transitions, at the point where merging occurs, the line photoexcitations are more than 10 times stronger than line collisional excitations and the free-bound excitations are more than 100 times stronger than the corresponding free-bound collisional excitations. Thus, the diffusion of photons in frequency is strong, i.e., there are many photon-scatterings per collisional excitation.

Near the surfaces of the 2-mm thick plasma where the flux patterns of the radiation begin to skew outward and become hemispheric, higher densities than $10^{22}$ cm$^{-3}$ are needed to bring the ion populations into LTE. Figures 6–9 illustrate this behavior in terms of the quantities in Eq. (31). These curves, of $\epsilon_\nu$, $(1-S_\nu^L/B_\nu)$, $(1-S_\nu^C/B_\nu)$, $F_\nu^L$, and $F_\nu^C$ were calculated at an ion density of

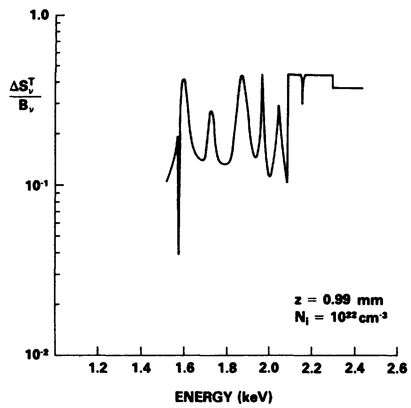


FIG. 6. The calculated percentage departure of the source function from blackbody values in the outer cell of the plasma is shown as a function of photon energy. The calculation was carried out at an ion density of $10^{22}$ $cm^{-3}$ and a plasma temperature of $5\times10^6$ K in a 2-mm thick plasma.

$10^{22}$ $cm^{-3}$ in the outside cell of the plasma. The center of this cell is located 0.99 mm from the plasma center. Figure 6 shows the frequency behavior of $\epsilon_\nu \equiv \Delta S_\nu^T/B_\nu$. Near the core of the satellite line, the source function approaches $B_\nu$ to better than 5%. At other frequencies, $S_\nu$ oscillates between 10 and 40% deviations from $B_\nu$ depending on which ionization stage and which emission process contributes most heavily to $S_\nu$. In Fig. 7, the separate contributions of $1 - S_\nu^L/B_\nu \equiv \Delta S_\nu^L/B_\nu$ and $1 - S_\nu^C/B_\nu \equiv \Delta S_\nu^C/B_\nu$ to $\Delta S_\nu^T/B_\nu$ are drawn for comparison to the $\Delta S_\nu^T/B_\nu$ curve. The $\Delta S_\nu^L/B_\nu$ curve is labeled BB and the $\Delta S_\nu^C/B_\nu$ curve, FB. One

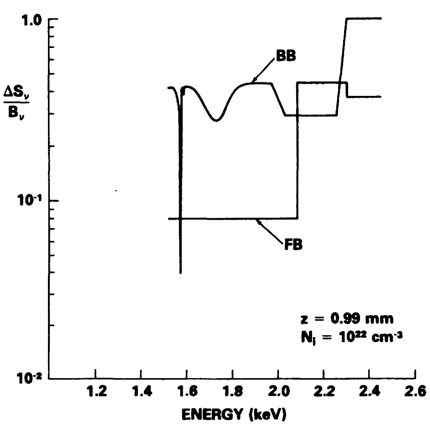


FIG. 7. The calculated percentage departures of the line source function (curve labeled BB) and the continuum source function (FB) from blackbody values in the outer cell of a 2-mm thick plasma is shown as a function of photon energy. The calculation was carried out at an ion density of $10^{22}$ $cm^{-3}$ and a plasma temperature of $5\times10^6$ K.

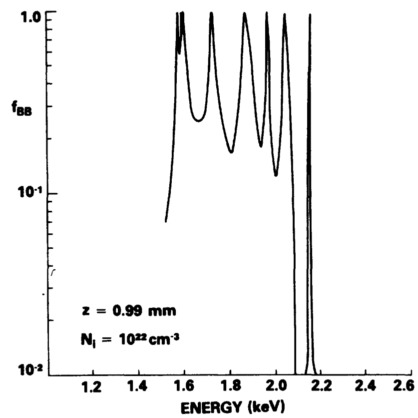


FIG. 8. The fraction by which the line source function of Fig. 7 contributes to the total source function of Fig. 6 is plotted as a function of photon energy.

can infer from Figs. 6 and 7 that the Al XIII system is closer to LTE than Al XII in agreement with Figs. 3 and 4, and that levels within Al XII and Al XIII deviate *uniformly* (i.e., by the same factor) from LTE. The fact that $S_\nu^L$ and $S_\nu^C$ are formed from sums of overlapping line and continuum emission processes can be seen from the way in which the two curves transit between the different line and continuum values. The weighting factors $F_\nu^L$ and $F_\nu^C$ (labeled $f_{BB}$ and $f_{FB}$, respectively) of the $\Delta S_\nu^L/B_\nu$ and $\Delta S_\nu^C/B_\nu$ contributions to $\epsilon_\nu$ are plotted in Figs. 8 and 9. In the region of overlap between the lines, far removed from the line cores, we see that photons are absorbed principally by photoionization events (80–90%), but that absorption in the wings of the highly broadened lines is still at minimum 10 to 20% of all absorptions.

The broadening of the lines as a function of ion

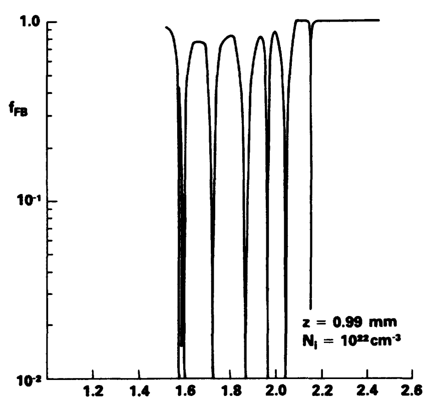


FIG. 9. The fraction by which the continuum source function of Fig. 7 contributes to the total source function of Fig. 6 is plotted as a function of photon energy.

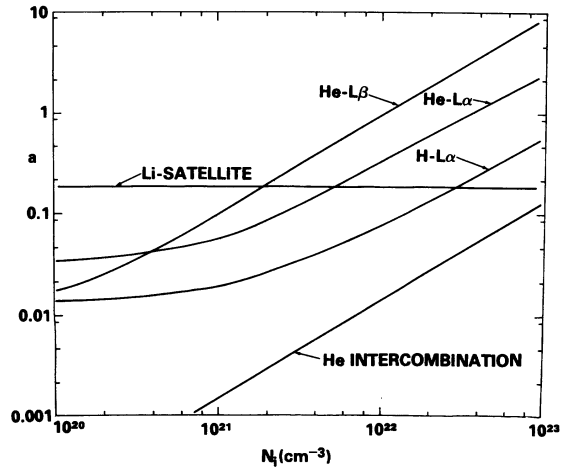


FIG. 10. The computed Voigt profile function parameter, $a$, which gives the ratio of collisional to Doppler linewidths, is plotted as a function of ion density for 5 of the lines in the $K$-series spectrum. The plasma was 2-mm thick and at a temperature of $5 \times 10^6$ K.

density is shown in Fig. 10, in which the Voigt profile parameter, $a$, is plotted for 5 of the transported lines. In these calculations, the Li-satellite linewidth is density independent, since it is the rate of autoionization that determines the collisional lifetime of the $1s2p^2$ level. Note that the He-like $L\beta$ line is more strongly broadened than the He-like $L\alpha$ line once collisional broadening becomes dominant since as one moves higher in the manifold of excited states, the state density becomes greater and the energy separation of the states becomes smaller leading to stronger collisional mixing and stronger interuptions of the radiative processes.

One result of the large broadening of the lines at high densities is that their opacities relative to the free-bound continuum decrease as the ion density is increased. This effect is seen in Fig. 11 where the optical depths of the two Lyman-$\alpha$ lines close to line center[10] are plotted as a function of ion density along with the free-bound optical depth at the emission edge of the $Z \rightarrow H$ and $H \rightarrow He$ ground-state-to-ground-state recombinations. In spite of the fact that the He – $L\alpha$ line opacity exceeded $10^5$ at the end of the calculations, they were performed for a fixed set of cell spacings that were finer toward the surface of the plasma. For example, the innermost cell was taken to be 400-$\mu$m thick, while the outermost cell was only 10-$\mu$m thick. Consequently, the spatial variations of the source function were imperfectly resolved as a function of density, i.e., optical depth; however, this is an intrinsic limitation of all radiation transport calculations that are based on a finite number of plasma cells.

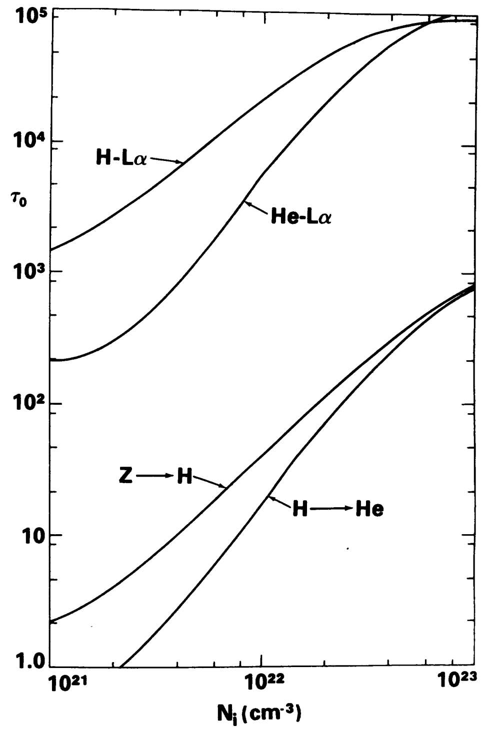


FIG. 11. The optical depths of the hydrogenlike and heliumlike Lyman-$\alpha$ lines near line center and of the $Z \rightarrow H$ and $H \rightarrow He$ ground-state radiative recombinations at the emission edge are plotted as a function of ion density. The plasma was 2-mm thick and at a temperature of $5 \times 10^6$ K.

When a different set of cell spacings were used to carry out the calculations, the photocouplings and emission spectra were changed somewhat, but not in a way to significantly affect the main conclusions or basic results of the calculations.

One of these basic results is the computed behavior of the emission spectrum as a function of ion density. Figures 12 and 13 contain 2 sets of spectra, at two different ion densities, of both the emergent flux and a blackbody flux calculated at the surface of the plasma (lower curves) and at 145 $\mu$m behind the surface (upper curves). Once again, these are spectra from 2-mm thick plasmas. The two sets of companion curves demonstrate a well-known phenomenon of line formation in a highly optically thick medium; namely, that line cores become self-absorbed in the surface layers of the emission region where the population can no longer be held in LTE by the decreasing strength of the radiation field as they are in the interior.[11] As can be seen in these figures, the spectrum at the points of reversal is also lowered from the blackbody curve. Figures 12 and 13, also illustrate how the $K$-shell spectrum changes from emission to absorption due to line-core

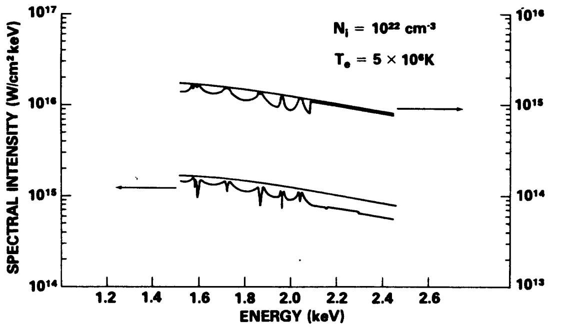


FIG. 12. The computed $K$-series emission spectrum from a 2-mm thick planar plasma at a density of $10^{22}$ ions/cm$^3$ and a temperature of $5 \times 10^6$ K is shown relative to the blackbody spectrum (lower set of curves). The same spectra as computed 145 $\mu$m behind the surface of the plasma are shown in the upper set of curves.

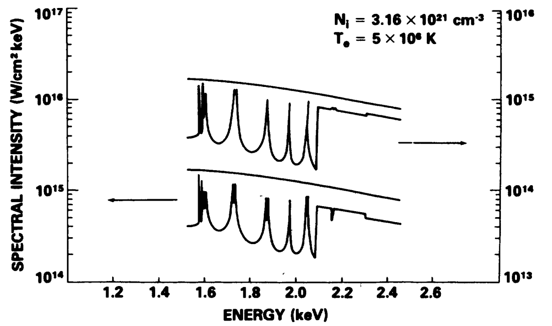


FIG. 13. The computed $K$-series emission spectrum from a 2-mm thick planar plasma at a density of 3.16 $\times 10^{21}$ ions/cm$^3$ and a temperature of $5 \times 10^6$ K is shown relative to the blackbody spectrum in the lower set of curves. The same spectra as computed 145 $\mu$m behind the surface of the plasma are shown in the upper curves.

reversal as the ion density is increased and the continuum and line wings move up toward the blackbody curve. The range of density values over which the plasma will produce an absorption spectrum is imperfectly predicted by these calculations since more cells are needed at the plasma surface to monitor the transition of the surface ionization state towards LTE when the plasma becomes collisionally dominated. One can infer from Fig. 5 that densities of at least $10^{24}$ are needed for this to occur. Note also in Fig. 13 that the lithiumlike satellite line is relatively unaffected by its passage through the surface layer, since its formation is already collisionally controlled by dielectronic recombination and autoionization. The relative populations of the two levels involved in this transition are determined essentially by the electron temperature; absorption in the continuum accounting for the remainder of the line-formation behavior (see Figs. 6–9).

$K$-shell spectrum formation at high density has several other interesting features. At $10^{22}$ ions/cm$^3$, for example, the Z $\rightarrow$ H and H $\rightarrow$ He continua are sufficiently opaque (Fig. 11) to become self-absorbed, like the line cores, on their passage through the surface layer. At $3.16\times10^{21}$ ions/cm$^3$, H $\rightarrow$ He emission is becoming thin, while Z $\rightarrow$ H emission remains relatively thick. Consequently, both the H-like $L\gamma$ line and the Z $\rightarrow$ H emission edge appear as absorption features in the H $\rightarrow$ He continuum. Finally, note that, while all the lines in Fig. 13 have opacities larger than 20, the $K$-shell spectrum lies completely away from the blackbody curve due to core self-absorption and continuum absorption.

Spatial differences in the ionization state of a

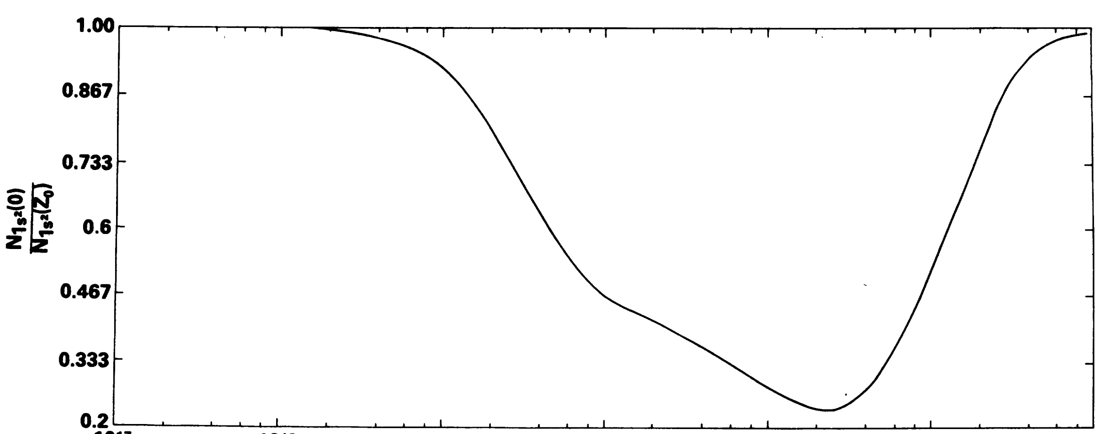


FIG. 14. The computed ratio of Al XII $1s^2$ $^1S$ population densities at the center and surface ($z = Z_0$) of the plasma is plotted as a function of ion density. The 2-mm thick plasma was at a temperature of $5 \times 10^6$ K.

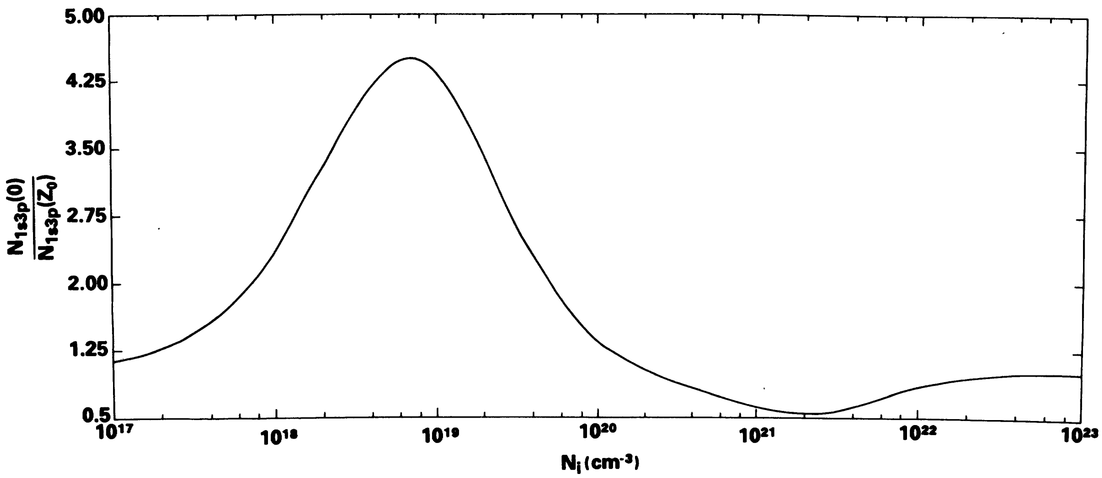


FIG. 15. The computed ratio of Al XII $1s3p\,^1P$ population densities at the center and surface ($z=Z_0$) of the plasma is plotted as a function of ion density. The 2-mm thick plasma was at a temperature of $5\times10^6$ K.

plasma of uniform temperature and density are induced by the radiation interactions. These ionization gradients can be inferred from the emission spectrum when line reversals are observed. However, the magnitude of the population differences is computable directly. Three examples are given in Figs. 14–16. The ratios of the population densities at the center and surface of the plasma of the heliumlike $1s^2$ ground state, $1s3p$ excited state, and the hydrogenlike $n=2$ excited state are shown in Figs. 14, 15, and 16, respectively, as a function of ion density. They were calculated over six orders of magnitude of density change in two separate calculations; one calculation was begun at the lowest, and, the other, at the highest density value in the figures. The self-consistency of the two calculations was demonstrated by their smooth merging at the density midpoint of $10^{20}$ ions/cm$^3$. The behavior of the ground state of Al XIII and of the Al XIV population density is similar to the behavior of the $1s3p$ and $n=2$ populations, respectively. Maximum gradients in the hydrogenlike and heliumlike excited-state manifolds occur at around $10^{19}$ ions/cm$^3$ while the maximum gradient in the heliumlike ground state occurs above $10^{21}$ ions/cm$^3$. At these maxima, from 4 to 7 times as many ions may exist at the center or surface of the plasma as exist at the surface or center, respectively.

## V. TEMPERATURE DIAGNOSTICS

One important reason for calculating x-ray emission from optically thick aluminum plasmas

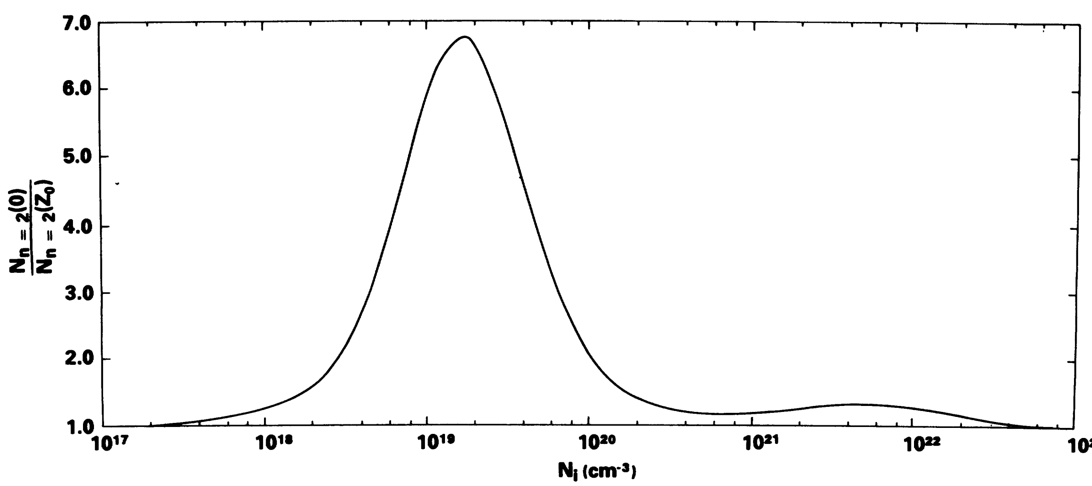


FIG. 16. The computed ratio of Al XIII $n=2$ population densities at the center and surface ($z=Z_0$) of the plasma is plotted as a function of ion density. The 2-mm thick plasma was at a temperature of $5\times10^6$ K.

of well defined sizes, shapes, ion densities, temperatures, and ionization states is that it is common experimental practice either to assume or to infer such information from x-ray spectral data obtained from laboratory experiments where the plasmas generated are short-lived ($\lesssim 0.1\ \mu$sec) and small ($\lesssim 1$ mm).[12] If the size and temperature of the emission region are known, as they were in the preceding calculations, the strength of the line reversals, the relative strengths of the continuum background to the line, linewidths, the height of collisionally controlled satellite lines, and the existence of absorption features in the continuum background all provide important density information about the medium. On the other hand, if the size and density of the emission region are known, the problem of deriving "a temperature" from spectral data appears to be much more complicated.

To begin with, in most laboratory situations, it is generally impossible to sustain the plasma in a steady state at a reasonably well-defined temperature, hence, the plasma's temperature will at first be rising and later falling (perhaps rapidly) during emission, and an assumption of collisional-radiative equilibrium may itself be of limited validity. Furthermore, the peak temperature reached may often be a function of the rates of heating and radiative cooling. Since time-integrated spectra are usually measured during short-lived experiments, variations of the emission spectrum with temperature must be known in order to properly time integrate different spectral features. In addition, most spectra are recorded on film, which generally has a dynamic range on the order of 100. Thus, it may not always be possible to simultaneously resolve the line and continuum structure. This recording problem is illustrated in Figs. 17 and 18.

Both spectra in Figs. 17 and 18 were calculated from a 2-mm thick planar plasma. The spectrum in Fig. 17 was calculated at an ion density of $3.16\times10^{19}$ cm$^{-3}$ and an electron temperature of $5\times10^{6}$ K, while, in Fig. 18, the ion density and electron temperature were $10^{20}$ cm$^{-3}$ and $1.88\times10^{7}$ K, respectively. In both figures, a dashed horizontal line is drawn, roughly 50 to 100 intensity units below the peak line intensity of each figure. In Fig. 17, none of the free-bound continuum lies above this line; in Fig. 18, only a small portion does. Film recordings of these spectra, therefore, would not necessarily detect any of the continuum background unless they were saturated at the lines.

The absolute intensities of the lines, and the relative intensities of the satellite to intercombination to resonance lines can be used to provide other spectral diagnostic information which is

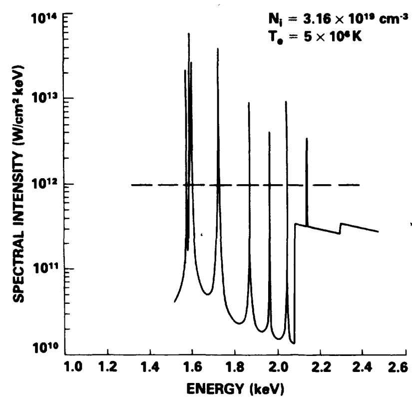


FIG. 17. Calculated $K$-series aluminum spectrum from a 2-mm thick plasma at an ion density of $3.16\times10^{19}$ cm$^{-3}$ and a temperature of $5\times10^{6}$ K.

sensitive to the temperature and opacity of the emission region. The intercombination line in Fig. 17, for example, is twice as intense as it is in Fig. 18; whereas, the resonance lines of Fig. 17 is more than 5 times as weak as it is in Fig. 18. Moreover, the intensity ratios of the satellite, intercombination, and resonance line are usually observed as they appear in Fig. 18.[13]

If line ratios are used to make temperature estimates of an optically thick transient emission region, it will be undoubtably important to locate the background continuum relative to the line peaks as well as to know the size of the emission region in order to have good estimates of both the density of the medium and of the relative amounts of collisional and opacity broadening of the lines. Figure 19 provides some information about these aspects of the problem of spectral interpretation. In this figure, seven calculated power output curves are drawn (per a unit of surface area) as a function of the plasma temperature for two cases

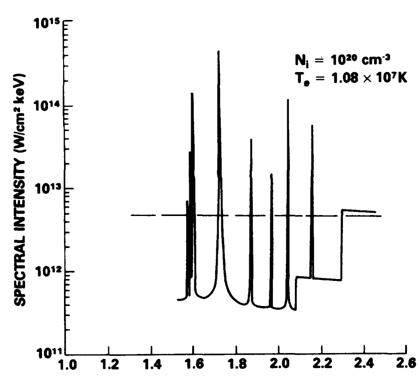


FIG. 18. Calculated $K$-series aluminum spectrum from a 2-mm thick plasma at an ion density of $10^{20}$ cm$^{-3}$ and a temperature of $1.08\times10^{7}$ K.

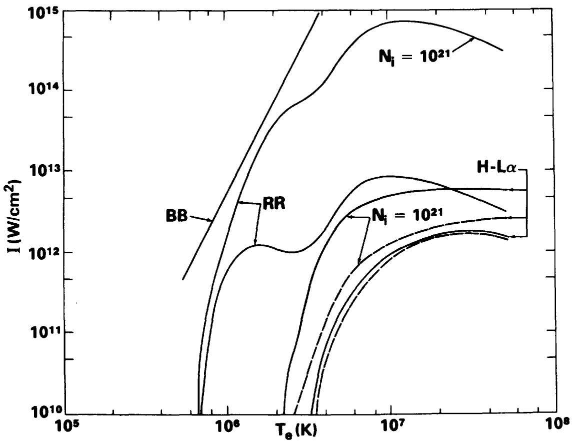


FIG. 19. The spectrally integrated intensity from a blackbody emitter (BB) is compared to the calculated integrated $K$-series emission into the continuum (RR) and hydrogen Lyman-$\alpha$ line (H $L\alpha$) from 2-mm thick plasmas at ion densities of $10^{20}$ cm$^{-3}$ and $10^{21}$ cm$^{-3}$. The solid H $L\alpha$ curves represent integrations of the line emission further into the wings of the line than the dashed H $L\alpha$ curves.

in which the ion density was $10^{21}$ cm$^{-3}$ and $10^{20}$ cm$^{-3}$. Again the plasma thickness was 2 mm. The curves labeled RR represent the integrated intensity under the $K$-shell spectrum (from 440 eV to 6.1 keV) exclusive of line-core radiation. Four curves of intensity output from the H $-$ $L\alpha$ line are also drawn; the dashed curves represent symmetrical integrations of the intensity under this line to 2.3 average Doppler widths ($7.25\times10^{13}$ Hz) from line center (which is at $4.17\times10^{17}$ Hz); the solid curves are integrations to 17.8 Doppler widths. At $10^{20}$ ions/cm$^3$, the dashed and solid curves of H $-$ $L\alpha$ emission are nearly identical and indicate that little emission occurs in the wings of this line; however, at $10^{21}$ ions/cm$^3$ the dashed and solid curves show there is considerable emission in the wings of the H $-$ $L\alpha$ line. The final curve on the figure, labeled BB, is a plot of the $\sigma T_e^4$ blackbody emission rate. The closeness of approach of the total $K$-shell emission curve at $10^{21}$ ions/cm$^3$ to the blackbody curve indicates the strength of the continuum emission from the He$\rightarrow$Li recombination in the sub-kilovolt spectral range. Per cm$^2$ of surface area, an input power of 10 TW would be needed to sustain a plasma of this size and density at temperatures around 300 to 400 eV against its x-ray energy loss.

If one compared experimentally only the intensity output curves of the H $-$ $L\alpha$ emission at the two densities of Fig. 19 one would overlook the approximate $N_i^2$ increase in $K$-shell x-ray yield due to the rise in continuum emission from the plasma. At $10^{20}$ ions/cm$^3$, our calculations show that continuum emission from the $K$ shell dominates over the line emission, although a film recording of this x-ray spectrum might indicate strong line and virtually no continuum emission. The reason for this recording phenomenon can be found in the relative sizes of the frequency intervals encompassed by the lines and by the continuum. For example, the frequency interval over which the solid emission curves of the $H\alpha$ line in Fig. 19 were computed was $2.67\times10^{15}$ Hz. On the other hand, the total frequency interval that is covered in our $K$-shell spectrum calculations is $1.37\times10^{18}$ Hz.

## VI. PHOTOPUMPING

We have seen that for 2-mm thick, planar aluminum plasmas photoabsorption is the dominant means of exciting the $K$ shell (see Fig. 5) at moderate densities and temperatures ($10^{19}\leq N_i \leq 10^{22}$, $T_e\sim5\times10^6$). One might expect, therefore, to produce a population inversion within the aluminum $K$ shell by selective photoexcitation. In fact, a scheme in which the $1s^2$-$1s2p$ resonance line in silicon is used to pump the $1s^2$-$1s3p$ transition in aluminum was proposed recently.[14]

One method of studying this proposal in its most ideal form is to pump a planar aluminum plasma symmetrically at both surfaces with a blackbody flux of photons that is filtered outside of a frequency interval surrounding the $1s^2$-$1s3p$ line at frequency $\nu_0$. The strength of the pump radiation can then by characterized by a radiation temperature $T_{\text{pump}}$, where

$$I_\nu^{\text{pump}} \equiv \frac{2h\nu^3/c^2}{e^{h\nu/kT_{\text{pump}}}-1}$$

for $\nu\in[\nu_0-\Delta\nu,\nu_0+\Delta\nu]$. $I_\nu=0$ otherwise. If the thickness of the aluminum plasma is sufficiently small and its density is sufficiently low, the pump radiation will penetrate the medium and produce an inversion between the $1s2p$ and $1s3d$ states in Al XII. Results from such a calculation are shown in Figs. 20–23. The calculation was carried out for the following uniform set of plasma conditions. The electrons were relatively cool for $K$-shell excitations at $2\times10^6$ K. The ion density was $2\times10^{19}$ cm$^{-3}$, and the aluminum plane was 1-mm thick, i.e., the distance the pump radiation has to penetrate to invert all of the Al XII populations was 500 $\mu$m. The gain coefficient for the $1s2p\,{}^1P$-$1s3d\,{}^1D$ line was calculated assuming no feedback on the population densities from this line radiation.

Figure 20 shows the computed emergent flux from the plasma when the strength of the pump radiation is defined by $T_{\text{pump}}=1.58\times10^6$ K, slightly

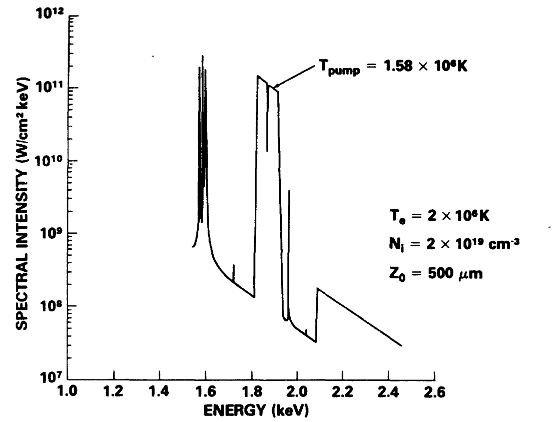


FIG. 20. Calculated $K$-series emission spectrum from a 1-mm thick plasma at an ion density of $2\times10^{19}$ cm$^{-3}$ and a temperature of $2\times10^6$ K in the presence of an external, filtered, blackbody pump of $1.58\times10^6$ K strength.

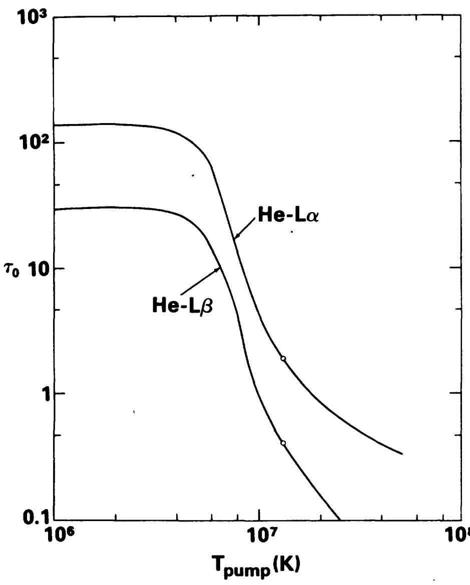


FIG. 22. Calculated optical depths of the heliumlike Lyman-$\alpha$ and Lyman-$\beta$ lines near line center and at plasma center as a function of pump strength.

below the ambient electron temperature. The frequency interval, $2\Delta\nu$, is sufficiently small so that only the $1s^2$-$1s3p$ line is pumped. The strength of the pumping is indicated by the depth of the hole in the pump radiation spectrum following its passage through the relatively cool plasma.

At a slightly higher blackbody pump temperature, the Al XII ions at the plasma surface acquire a $1s2p$-$1s3d$ inversion (see Fig. 21). The gain coefficient rises steeply to a value of 50 cm$^{-1}$ at a pump "temperature" 3 times the electron temperature. However, $T_{pump}$ must reach values in excess of $10^7$ K in order for the pump radiation to sufficiently penetrate the plasma to invert the $1s2p$ and $1s3d$ states in the center cell and to generate an integrated gain $G\equiv\int_0^{z_0} g\,dz$ in the direction perpendicular to the surface. [Because of the thickness of the center cell in these calculations (150 $\mu$m), the rise in $G$ followed closely the rise in $g(z=0)$.]

The behavior of $G$ is correlated to the behavior of the optical depths at the center of the plasma of the $1s^2$-$1s2p$ and $1s^2$-$1s3p$ lines, which are shown in Fig. 22 as a function of $T_{pump}$. Below $8\times10^6$ K, the optical depth of the He-$L\beta$ line is too large for much of the pump radiation to pene-

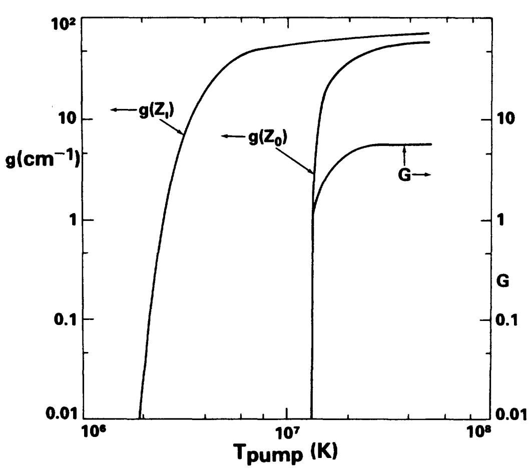


FIG. 21. The calculated gain coefficient at the surface of the plasma ($z=Z_1$) and near the center of the plasma ($z=Z_0$) is shown as a function of the strength of the external pump radiation. The integrated gain in the direction perpendicular to the plasma surface is also drawn.

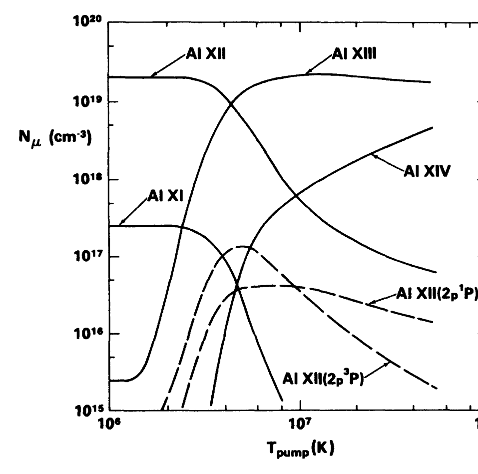


FIG. 23. Calculated population densities at the surface of the plasma as a function of the strength of the external pumping radiation. The electron temperature in the plasma was $2\times10^6$ K.

trate into the plasma. At $T_{pump} \gtrsim 10^7$ K, the He-$L\beta$ optical depth finally drops to one and the plasma center volume is pumped; however, self-absorption of the He-$L\alpha$ line is still sufficiently high to populate the $1s2p$ state and quench the $1s2p$-$1s3d$ inversion. A further increase in the pump strength is needed to diminish He-$L\alpha$ absorption and invert the $1s2p$-$1s3d$ populations in the plasma interior.

The decrease in opacity of the Al XII Lyman lines with pump strength is related to the dual effect of this radiation to populate the upper energy levels and to deplete the heliumlike ground state of the aluminum plasma in CRE. These effects are illustrated in Fig. 23, where the population densities of the Al XI through Al XIV ground states and the $1s2p\,^1P$ and $1s2p\,^3P$ excited states at the plasma surface are plotted as a function of $T_{pump}$. At a plasma temperature of $2\times10^6$ K and for $T_{pump} \le 10^6$ K, the plasma consists mainly of the ground state of Al XII and is primed for pumping. As $T_{pump}$ is increased, Al XII is excited to the $1s2p\,^1P$ state, where electron collisions are sufficiently energetic and frequent to populate other excited levels in Al XII as well as the ground state of Al XIII. When Al XIII decays radiatively to the Al XII ground state, the emitted free-bound continuum acts to pump the $n=3$ state in Al XIII. Electron collisions ionize this state and Al XIV ions are formed. Also, once $1s2p\,^3P$ states are produced through collisional mixing of Al XII excited states, they become photoionized by the pump radiation, i.e., the $1s2p\,^3P$ state is the only excited state in Al XII that is photocoupled to Al XIII in our present analysis. Hence, the more rapid fall of the $1s2p\,^3P$ than the $1s2p\,^1P$ population density with increasing $T_{pump}$ is an artifact of our model.

## VII. SUMMARY AND CONCLUSIONS

In recent years, several new experimental methods have been developed to generate high-energy-density plasmas in the laboratory, two of the most notable being laser produced and exploding wire plasmas.[15] While they are similar in many ways to astrophysical plasmas, these laboratory plasmas differ in two important respects from their astrophysical counterparts. One, they are highly transient, and two, their sizes are of the order of x-ray absorption lengths. Hence, during the course of their evolution, they enter and leave regimes where the frequency-by-frequency opacity of the radiation they generate enter significantly into the physics of their evolution.

Because of the similarities of plasma conditions, however, it is natural that the techniques of x-ray data analysis, commonly employed in astrophysics, should be utilized to aid in the interpretation of the x-ray data that is being acquired in the laboratory. However, because of the important space-time differences, the x-ray analysis techniques of astrophysics must also be refined and further developed to be applied with the required generality as a laboratory analysis tool.

In the calculations that were described in this paper, the photocoupling physics was an integral element of not only the energy flow within small, highly excited, dense aluminum plasmas, but of the excitation states of these plasmas as well. We were able, nevertheless, to self-consistently compute the aluminum $K$-shell emission spectrum in a simple planar geometry and to thereby establish that techniques can be developed to analyze theoretically generated x-ray spectra in analogy to the techniques that are used to analyze experimental spectra, e.g., densitometry, the measurement of line ratios, widths, etc. The advantage in the theoretical case, of course, is that all of the underlying conditions of the emitting medium are known and can be monitored directly. In fact, we have also made movies which demonstrate in time, for example, how the spectra of Figs. 12 and 13 slowly evolve into one another as the ion density is changed. To paraphrase from Scott's article,[16] just as the graphical display of data, which replaced the tabulation of numbers, was a major past scientific advancement, similar benefits may occur as scientific movie making allows one to correlate changes of these graphical data displays in time. Since the variability of plasma conditions is very large, simple physical systems must be analyzed, at first, before one can progress sensibly in directions of more complex physical situations. For this reason, the plasma conditions that were used in the calculations of this paper were purposely chosen to be uniform.

Four important effects were seen as the ionization stages of the $K$ shell approached LTE and the plasma approached radiative equilibrium. First of all, in a millimeter sized aluminum plasma, the LTE approach is made under conditions where, for example, photo-excitation rates are 10 to 100 times larger than corresponding collisional excitation rates. Secondly, the collisional widths of the lines begin to exceed their Doppler widths as the $K$-shell emission spectrum approaches the blackbody curve. Broadly self-absorbed line cores result and the line emission begins to strongly overlap. At frequencies midway between the lines, where normally one expects continuum emission to dominate, the lines account for 10 to 20% of the source function. Thirdly, in contradistinction to the two-level atom approximation, which is often used in astrophysics at low ion densities and low x-ray fluence levels, the quenching contributions of collisional transitions to and from levels outside of the two undergoing the radiative transition were found to have an equal influence, along with the photocouplings, on the rate of approach of the population densities to LTE. Finally, the ability of spatial gradients in the energy density of the radiation field to induce spatial gradients in the population densities was found to extend over at least 6 to 7 orders of magnitude in ion density.

Two calculations were also described where the plasma temperature was varied at two different fixed ion densities and where continuum emission in the $K$ shell was found to increase as $N_i^2$ while the corresponding line emission increase was less than $N_i$ (Fig. 19). In these calculations, continuum emission was found to exceed line emission (at ion densities $\gtrsim 10^{20}$ cm$^{-3}$). Moreover, at $10^{21}$ ions/cm$^3$, continuum emission totally dominated the energy flow from the plasma and approached the rate of blackbody emission at temperatures around $2\times10^6$ K, where He $\rightarrow$ Li recombination was the major emission process. The inclusion of $L$-shell radiation into the calculation will no doubt lead to the conclusion that aluminum at the plasma conditions of this calculation is a blackbody radiator.

The importance of the continuum background was seen for both temperature and density diagnostics even though on film this measurement may be difficult. Because of the time-dependent nature of x-ray emission processes in the laboratory, a "temperature estimate" of the plasma from x-ray data, if based on considerations other than an energy-level diagram, might easily be meaningless or at best misleading. This statement will be especially true if the size and density of the emission region are changing with time in addition to the temperature.

Finally, in order to more dramatically illustrate the radiation field's ability to drive the aluminum $K$ shell, a calculation was performed in which the $1s^2$-$1s3p$ transition in Al XII was pumped by an idealized external source that was designed to produce an inversion of the $1s2p\,^1P$ and $1s3d\,^1D$ states. The results of the calculation suggested that x-ray lasers based on x-ray optical pumping schemes may need to be designed as surface lasers[17] if CRE conditions are approximated and opacity effects are important. We found in the test situation under study that, as the pump strength was increased, the gain coefficient at the surface of the plasma saturated. This effect was caused by the depletion of the Al XII ground state as the pump radiation penetrated further into the plasma. In fact, beyond equivalent blackbody pump strengths of twice the background electron temperature, the ionization of the $K$ shell was determined as much by the pump photons that bathed these ions as by the ambient electron gas.

## ACKNOWLEDGMENT

This work was supported by the Defense Nuclear Agency.

[1]D. H. Sampson, *Radiative Contributions to Energy and Momentum Transport in a Gas* (Interscience, New York, 1975).

[2]J. Davis and K. G. Whitney, J. Appl. Phys. 47, 1426 (1976).

[3]V. Jacobs and M. Blaha, Phys. Rev. A 21, 525 (1980).

[4]J. Davis, K. G. Whitney, and J. P. Apruzese, J. Quant. Spectros. Radiat. Transfer 20, 353 (1978).

[5]S. Chandrasekhar, *Radiative Transfer* (Dover, New York, 1960), p. 12.

[6]D. Mihalas and P. B. Kunasz, Astrophys. J. 219, 635 (1978).

[7]For simplicity, the $\nu^{-1}$ dependence of the free-bound emission profile was neglected along with Gaunt factor frequency dependences.

[8]M. Seaton, Mon. Not. R. Astron. Soc. 119, 81 (1959).

[9]Two approximations were involved in this procedure. The lifetimes of the lower states were ignored and, in Al XIII, mixing rates between the degenerate levels were not calculated and hence the identification of the lifetimes of the radiating substates was not made.

[10]Our frequency grid did not include exact line-center frequencies, so, for convenience, line optical depths were computed at those frequencies which lay closest to the line centers.

[11]E. H. Avrett and D. G. Hummer, Mon. Not. R. Astron. Soc. 130, 295 (1965); D. G. Hummer, *ibid.* 138, 73 (1968).

[12]P. Burkhalter, J. Davis, J. Rauch, W. Clark, G. Dahlbacka, and R. Schneider, J. Appl. Phys. 50, 705 (1979).

[13]These theoretical spectra will generally not be observed as shown in Figs. 17 and 18 depending on the amount of instrumental or source broadening, i.e., the narrow satellite and intercombination lines of Fig. 17 will also generally be observed to be much less intense than the resonance line as they are in Fig. 18.

[14]A. V. Vinogradov, I. I. Sobelman, and E. A. Yukov, Kvant. Electron. (Moscow) 2, 105 (1975) [Sov. J. Quantum Electron. 5, 59 (1975)]; see also J. P. Apruzese, J. Davis, and K. G. Whitney, J. Phys. B 11, L643 (1978).

[15]P. Burkhalter *et al.*, Ref. 12; K. B. Mitchell, D. B. van Husteyn, G. H. McCall, P. Lee, and H. R. Griem, Phys. Rev. Lett. 42, 232 (1979); B. Yaakobi, D. Steel, E. Thorsos, A. Hauer, and B. Perry, Phys. Rev. Lett. 39, 1526 (1977); C. M. Lee and A. Hauer, Appl. Phys. Lett. 33, 692 (1978).

[16]J. T. Scott, Phys. Today 32, No. 1, 46 (1979).

[17]F. Varsanyi, Appl. Phys. Lett. 19, 169 (1971).